Spatial distribution of Northern Hemisphere winter temperatures during different phases of the solar cycle

V. Maliniemi[1], T. Asikainen[1], and K. Mursula[1]

[1] ReSoLVE Centre of Excellence, Department of Physics, University of Oulu, Oulu, Finland

Abstract Several recent studies have found variability in the Northern Hemisphere winter climate related to different parameters of solar activity. While these results consistently indicate some kind of solar modulation of tropospheric and stratospheric circulation and surface temperature, opinions on the exact mechanism and the solar driver differ. Proposed drivers include, e.g., total solar irradiance (TSI), solar UV radiation, galactic cosmic rays, and magnetospheric energetic particles. While some of these drivers are difficult to distinguish because of their closely similar variation over the solar cycle, other suggested drivers have clear differences in their solar cycle evolution. For example, geomagnetic activity and magnetospheric particle fluxes peak in the declining phase of the sunspot cycle, in difference to TSI and UV radiation which more closely follow sunspots. Using 13 solar cycles (1869–2009), we study winter surface temperatures and North Atlantic oscillation (NAO) during four different phases of the sunspot cycle: minimum, ascending, maximum, and declining phase. We find significant differences in the temperature patterns between the four cycle phases, which indicates a solar cycle modulation of winter surface temperatures. However, the clearest pattern of the temperature anomalies is not found during sunspot maximum or minimum, but during the declining phase, when the temperature pattern closely resembles the pattern found during positive NAO. Moreover, we find the same pattern during the low sunspot activity cycles of 100 years ago, suggesting that the pattern is largely independent of the overall level of solar activity.

1. Introduction

Several studies have shown solar cycle related modulation of winter climate at high northern latitudes (for a review, see, e.g., *Gray et al.* [2010]). The solar cycle modulation has been observed as significant differences between solar maximum and minimum times in several atmospheric phenomena during the Northern Hemisphere winter. Such differences have been observed, e.g., in the polar temperatures and geopotential heights in the stratosphere [e.g., *Labitzke*, 2005] and in the troposphere [e.g., *van Loon and Labitzke*, 1988], in the Atlantic and European sea level pressure [*Brugnara et al.*, 2013], and the extension of North Atlantic oscillation (NAO) [*Kodera*, 2002], as well as the other low-frequency circulation modes [*Huth et al.*, 2006], in the persistence of blocking events [*Barriopedro et al.*, 2008] and in the occurrence of synoptic weather types over Europe [*Huth et al.*, 2008].

These studies defined the solar cycle and the respective maxima and minima in terms of the sunspot number (SSN) or the solar 10.7 cm radio flux, which correlate highly with the solar UV and the total solar irradiance (TSI). TSI has been known to vary only about 0.1% over the solar cycle [*Gray et al.*, 2010], and reconstructions of the past TSI show variations of similar magnitude on centennial time scales [e.g., *Krivova et al.*, 2010]. However, different spectral bands in the solar spectrum, especially UV, can have a much larger relative variation over the solar cycle [*Ermolli et al.*, 2013].

The transfer of the solar UV signal from the upper/middle atmosphere to the surface can be explained by the top-down mechanism. Enhanced ozone levels and increased temperature in the equatorial and low-latitude stratosphere related to the increasing solar UV radiation strengthen the meridional temperature gradient and modulate the Brewer-Dobson circulation [*McCormack and Hood*, 1996]. This modulation is carried poleward and downward through the wave-mean flow interaction, ultimately causing changes in the high-latitude winter troposphere [*Kodera and Kuroda*, 2002; *Matthes et al.*, 2004, 2006]. Another suggested mechanism transferring the solar signal to the high-latitude surface in winter is the so-called bottom-up mechanism. Enhanced solar heating of the equatorial ocean surface during solar maximum increases

evaporation and transfer of latent heat to the upper troposphere/lower stratosphere. This increased heat is carried to the convergence zones by the trade winds, creating a positive feedback and ultimately also affecting the North Pacific and the Arctic sea level pressure [e.g., *Meehl et al.*, 2008]. Note that this mechanism has been criticized recently [*Roy and Haigh*, 2012].

Recently, it has also been proposed that changes in the UV radiation can affect with a considerable time lag. *Scaife et al.* [2013] showed in their coupled ocean-atmosphere model that a step-like change in solar UV forcing results in a change in the North Atlantic sea level pressure resembling positive NAO phase, which builds up during several years and attains the peak response 2–4 years after the change in UV forcing. The mechanism causing the lag was explained by the Atlantic Ocean acting as a heat buffer, which stores wintertime temperature anomalies into the ocean layers and feeds them back into the atmosphere during the next year. Such an ocean-atmosphere coupling, if strong enough, may create a lag of a few years between the change in UV forcing and the NAO response. *Gray et al.* [2013] discussed sea level pressure variability and showed that a positive type NAO response appears in the observations a few years after the solar cycle maximum. They also modeled the effect by using the same general circulation model as *Scaife et al.* [2013] but using a realistic solar cycle input based on observed sunspot number (instead of a step change in UV irradiance). Using this model they found the peak positive NAO response around the solar maximum. Both *Scaife et al.* [2013] and *Gray et al.* [2013] speculated that the ocean-atmosphere coupling in the model may not be strong enough to explain the observations.

Several recent studies have shown a clear relation between the Northern Hemisphere winter conditions and solar-related factors that are not well in phase with the sunspot cycle. These include geomagnetic activity, which has been found to correlate positively with the NAO index in recent years [*Thejll et al.*, 2003], and to cause significant surface temperature variations [*Rozanov et al.*, 2005; *Seppälä et al.*, 2009; *Baumgaertner et al.*, 2011]. *Bochníček and Hejda* [2005] showed that both solar and geomagnetic activity modulate the NAO pattern, but the effect of geomagnetic activity is stronger. *Woollings et al.* [2010] showed that there is a stronger and more consistent relationship between the open solar flux (derivable from geomagnetic data) and NAO than between $F_{10.7}$ cm and NAO. *Lockwood et al.* [2010] linked times of minimum open solar flux to the cold winters in Europe through blocking events. The cyclic variation of the open solar flux has about 1 year lag with respect to the TSI variation [*Lockwood et al.*, 2010]. Other studies have found that solar wind speed (V_{SW}) [*Boberg and Lundstedt*, 2003] or solar wind dynamic pressure [*Lu et al.*, 2008] affects the NAO variability. Recently, *Maliniemi et al.* [2013] showed that the energetic electron precipitation (EEP) into the atmosphere correlates significantly with surface temperature forming a pattern which strongly resembles the positive NAO temperature pattern [*Hurrell et al.*, 2003].

A proposed mechanism linking these drivers to winter circulation variability at polar regions involves energetic particle precipitation into the high-latitude atmosphere causing significant changes in atmospheric chemistry, e.g., by producing nitrogen oxides (NO_x) in the upper atmosphere [*Seppälä et al.*, 2007; *Sinnhuber et al.*, 2011]. NO_x in turn can descend down [*Funke et al.*, 2005] and affect ozone balance in the stratosphere during polar winter, when NO_x lifetimes are long due to the absence of sunlight and a large-scale downward motion exists in the polar atmosphere [*Randall et al.*, 2005; *Konopka et al.*, 2007]. *Baumgaertner et al.* [2011] stated that the polar stratospheric ozone loss strengthens the polar vortex and the northern annular mode (NAM). These NAM anomalies can also be observed on the surface [*Baldwin and Dunkerton*, 2001]. This mechanism is also well observed in the chemistry-climate models [*Rozanov et al.*, 2005; *Baumgaertner et al.*, 2011; *Rozanov et al.*, 2012].

Calisto et al. [2011] and *Rozanov et al.* [2012] found in their chemistry-climate models that galactic cosmic rays (GCR) cause ozone loss in the polar lower stratosphere and modulate trosheric temperatures during winter. *Veretenenko et al.* [2005] also linked long-term variations in the North Atlantic surface air pressure to the cosmic rays. *Mironova et al.* [2012] recently found an association between energetic electron precipitation and the vorticity of winter storms on the day-to-day time scale, which suggests a much faster mechanism than ozone destruction, possibly by the modulation of the global electric circuit [*Tinsley*, 2000].

Other studies have indicated that the above-mentioned mechanisms can act together by either enhancing or canceling each other depending on the level of solar or geomagnetic activity [*Lu et al.*, 2007]. *Seppälä et al.* [2013] found that strengthening of the stratospheric polar vortex by geomagnetic activity was stronger during high solar activity. *Bochníček et al.* [2012] found that during high solar and geomagnetic activity of recent years, the geopotential height anomalies in the troposphere resembled the positive NAO

anomaly, but most of the effect came from geomagnetic activity. *Li et al.* [2011] proposed that the relation between geomagnetic activity and NAO is nonlinear and nonstationary so that it is negative for weak to medium geomagnetic activity and positive for high activity, and that it depends on multidecadal variation in solar activity.

In this paper we study the dependence of the Northern Hemisphere winter surface temperatures and the NAO index on the sunspot cycle phase during the last 13 cycles (12 cycles for surface temperature). Due to the high correlation of the solar radiation related drivers (SSN, TSI, and UV flux), their effects cannot be distinguished from each other. On the other hand, the cyclic behavior of geomagnetic activity, solar wind speed, and energetic particle fluxes has been different from sunspots at least during the observed era, peaking in the declining phase of the sunspot cycle. Galactic cosmic rays are in the clear antiphase with the solar cycle peaking in the minimum phase of the solar cycle. The paper is organized as follows: In section 2 we will discuss the solar cycle and longer-term evolution of sunspots and other solar-related factors. Section 3 will give the details of the solar cycle phase function, which we will use as a tool to separate different cycle phases. Section 4 presents the results on surface temperature variability during the different phases of the solar cycle, and section 5 gives the results on NAO variability. In section 6 we will discuss the temperature variability in the different cycle phases during the considerably weak sunspot cycles in 1880–1925. Concluding remarks are made in section 7.

2. Evolution of Solar-Related Parameters

Figure 1 depicts the 3 month winter averages (December, January, and February) of sunspot numbers (obtained from Solar Influences Data Analysis Center http://sidc.oma.be/sunspot-data/), the *aa* index of geomagnetic activity (World Data Center archives http://www.ukssdc.ac.uk/wdcc1/data_menu.html), solar wind speed (NASA OMNIWeb database, http://omniweb.gsfc.nasa.gov/), EEP flux [*Asikainen and Mursula*, 2013], cosmic ray intensity (Oulu neutron monitor http://cosmicrays.oulu.fi/), and the NAO index (https://climatedataguide.ucar.edu/climate-data/hurrell-north-atlantic-oscillation-nao-index-station-based).

Figure 1 shows interesting features in the long-term variation of the different parameters. Sunspot activity shows the evolution of the Modern Grand Maximum during the twentieth century with the peak in cycle 19. Cycle 24 seems to remain the weakest cycle at least since the cycle 14. The *aa* index has been strengthening quite dramatically from 1900s to 1990s. The latest minimum depicts a noticeable decrease even in the *aa* index. It is also interesting that the correlation of the *aa* index with sunspots weakens during the latter half of the twentieth century with the *aa* index peaks moving later to the declining phase [*Echer et al.*, 2004; *Georgieva et al.*, 2006]. This probably indicates the growing tendency of polar field strength and polar coronal holes, enhancing the contribution of the associated high-speed solar wind streams to the *aa* index during this time. The other major contributions to the *aa* index are the coronal mass ejections peaking around the sunspot maximum.

Variation in the energetic electron precipitation (see fourth panel from top in Figure 1) follows best the variation in the V_{SW}. There are still some differences between the *aa* index and the EEP flux, e.g., in cycle peaks, which can deviate by up to 2 years. Therefore, caution is needed if geomagnetic activity is used as a proxy for energetic electron precipitation [*Maliniemi et al.*, 2013]. No clear long-term trend is seen in either V_{SW} or EEP flux until a clear decrease in cycle 23. GCR flux shows the well-known anticorrelation with sunspot cycle and the exceptional increase in the GCR amount during the last sunspot minimum as a response to the weaker heliospheric magnetic field since the declining phase of cycle 23 [*Smith and Balogh*, 2008; *Leske et al.*, 2013].

We have also displayed in Figure 1 the variation of the NAO index, which has been shown to significantly affect the winter surface temperature anomalies on the northern high latitudes [*Hurrell*, 1995; *Hurrell et al.*, 2003]. We note that the NAO index used here is station based (normalized pressure difference between the stations in Stykkisholmur/Reykjavik, Iceland and Lisbon, Portugal), which means that it is fixed in space. This is not ideal because of the movement of the pressure centers both annually [*Barnston and Livezey*, 1987] and longer [*Wang et al.*, 2012], but we use it here in order to have a longer temporal coverage, rather than using the NAO index obtained by principal component analysis which is only available during the twentieth century. Regardless, the correlation of station-based and principal component based NAO indices during winter months is very high [*Hurrell and Deser*, 2009]. Alternative would be to use sea level pressure data to
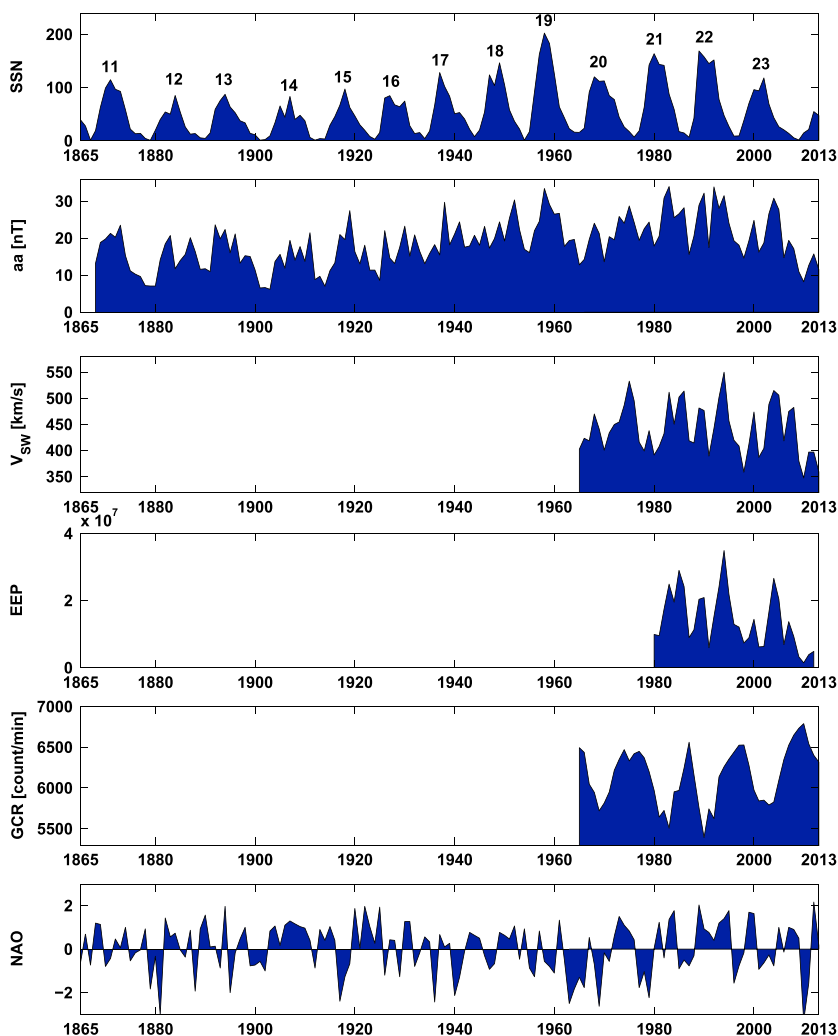
Figure 1. Mean winter values of (top to bottom) sunspot number (with corresponding cycle numbers), *aa* index, solar wind speed, EEP flux, galactic cosmic rays, and the NAO index. Values of EEP and NAO are normalized (unitless).

analyze the whole spatial extension of North Atlantic pressure field to see the movement related to the solar cycle [*Huth et al.*, 2006]. However, this is out of the scope of this paper; and thus, we keep it in mind when interpreting the main results.

3. Sunspot Cycle Phase Function

In this study we used the list of sunspot cycle maximum and minimum times determined by the National Geophysical Data Center (ftp://ftp.ngdc.noaa.gov/STP/space-weather/solar-data/solar-indices/sunspot-numbers/cycle-data/table_cycle-dates_maximum-minimum.txt) extended by including February 2012 as the estimated maximum of the cycle 24 (current maximum in the 13 month smoothed sunspot number). Using these minimum and maximum times we defined the sunspot cycle phase parameter as a function of time. For each solar cycle the phase of the sunspot minimum was defined to be 0° (modulo 360°) and sunspot maximum 180°. We then defined the monthly values (and the mean winter value) of sunspot cycle phase between minimum and maximum times linearly in time so that 90° will denote the center of the ascending phase of the cycle and 270° the center of the declining phase of the cycle. Note that we use only the sunspot cycle phases and do not take into account the relative height of the sunspot cycles.

The time series of the monthly values of the sunspot cycle phase function since 1868 is depicted in the top panel of Figure 2. One can see how the length of the cycles varies considerably over time. Cycles starting
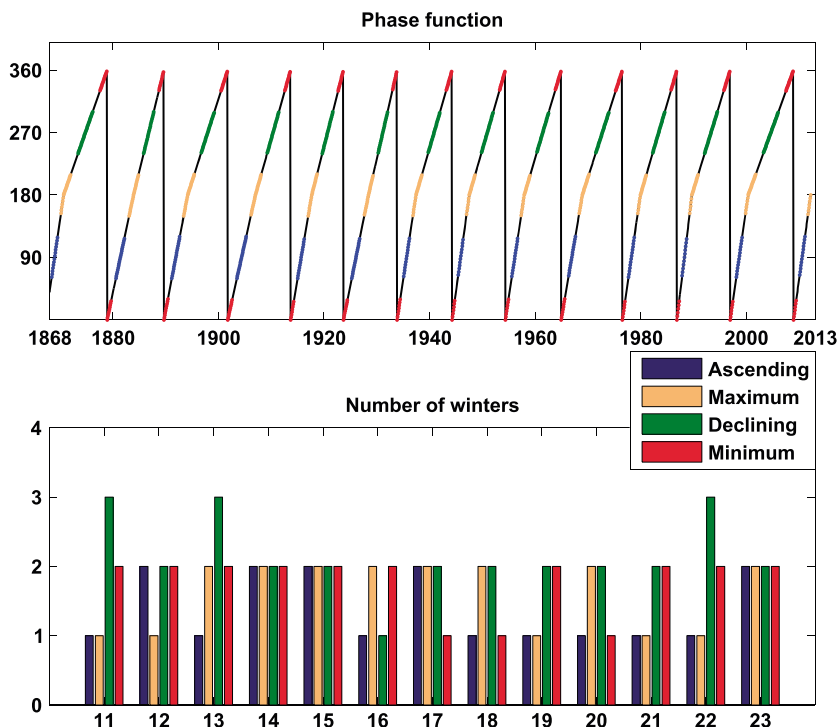
Figure 2. (top) Sunspot cycle phase function (whole year) since 1868. Each cycle phase extends 60° in phase and is denoted with a separate color. (bottom) Number of winters (December, January, and February) in each cycle phase for cycles 11 to 23.

from cycle 17 (after minimum in 1934) are systematically more asymmetric (having a longer time from maximum to minimum than from minimum to maximum) than the earlier, weaker cycles. Figure 2 also depicts the four cycle phases defined as 60° long windows of the sunspot phase function around the respective center of cycle phase (ascending phase 60°–120°, maximum phase 150°–210°, declining phase 240°–300°, and minimum phase 330°–30°). Cycle phase lengths were chosen to be 60° instead of 90° in order to obtain a better separation for the different cycle phases.

In total we have 13 full solar cycles starting from the ascending phase of cycle 11 in 1869 and ending to minimum in 2009 (exact sunspot minimum is in November 2008, but in our analysis the cycle minimum extends by 30° forward in the phase function). Note that the current sunspot maximum is not yet verified, and the length of the previous cycle minimum time can slightly change depending on the final date of the sunspot maximum. The lower panel of Figure 2 shows the number of winters (defined as December, January, and February) in each phase during each cycle. One can see that cycles 11, 13, 16, and 18–22 have relatively short ascending phases including only one winter, whereas the declining phases have contributions from at least two winters (except in cycle 16). In total we have 18 winters in the ascending phase, 21 in the maximum phase, 28 in the declining phase, and 23 in the minimum phase.

Figure 3 shows the mean winter values of different solar-related parameters as a function of the sunspot cycle phase. Each parameter has been normalized by subtracting its minimum value and dividing by the standard deviation of all values. (Note that solar wind speed, precipitating electrons, and cosmic ray values are calculated from shorter time periods than sunspot number and *aa*, as depicted in Figure 1.) These normalized winter values were then averaged in 30° phase bins, taking the bin center as the common time for all parameters. One can see that the sunspot number has the well-known double peak structure during maximum, and that the official definition of solar maximum occurs between these two. One can see that solar wind speed and EEP flux peak in the declining phase, and they have minimum after the sunspot minimum in the ascending phase. Both the solar wind speed and EEP flux drop quite sharply after their peak values toward solar minimum. Cosmic rays are in rather direct antiphase with the sunspot cycle.
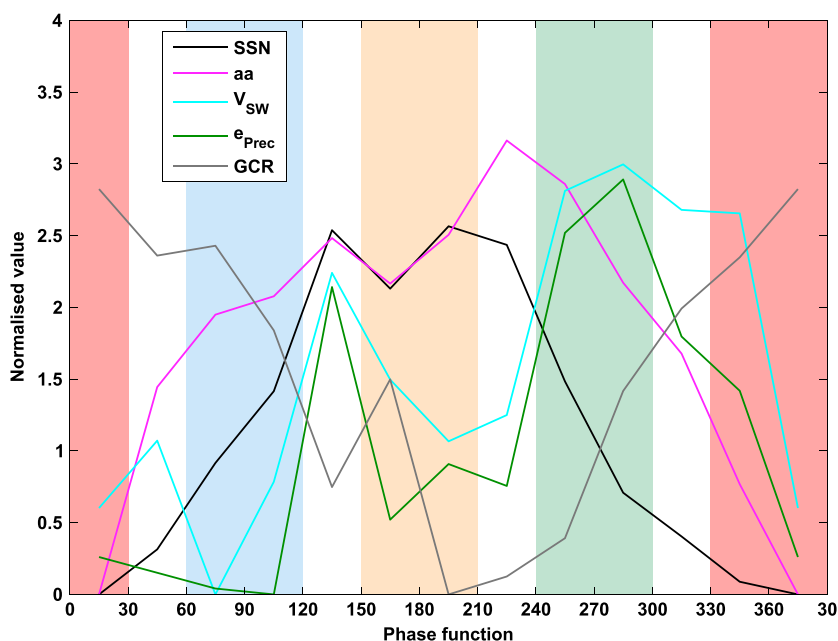
Figure 3. Mean winter values of (black) sunspot number, (magenta) *aa* index, (cyan) solar wind speed, (green) EEP flux, and (grey) cosmic rays distributed according to the sunspot cycle phase. The 60° wide cycle phases are colored similar as in Figure 2 but with lighter shading.

4. Temperature Anomalies During Different Phases of the Sunspot Cycle

Consistent surface temperature records covering roughly the whole Northern Hemisphere are provided from 1880 onward (NASA Goddard Institute for Space Studies surface temperature record http://www.esrl.noaa.gov/psd/data/gridded/data.gistemp.html). Temperature data are presented as gridded monthly temperature maps in 2° × 2° boxes of geographical latitude and longitude. They are constructed from ground station data of the Global Historical Climatology Network, from Hadley Centre analysis of sea surface temperatures (HadISST1) for 1880–1981 and from satellite measurements of sea surface temperature from 1982 onward (Optimum Interpolation Sea Surface Temperature Version 2). The temperature maps use spatial smoothing with a radius of 1200 km so that the temperature anomaly at a given location is computed as a weighted average of anomalies of all stations located within 1200 km of that point, with the weight decreasing linearly as a function of distance from one to zero at 1200 km distance (for more information on temperature data, see *Hansen et al.* [2010]).

We study here how the winter temperature anomalies vary in the different phases of the sunspot cycle. The surface temperature measurements cover 1880–2009, including 12 solar cycles. In each grid point we subtracted from the original data (monthly anomaly relative to the 1951–1980 base period) a smoothly changing trend so that the long-term temperature trend would not mask the possible cyclic variability. This trend was determined by filtering the data twice with a 31 year window separately for each month (before computing the winter averages) using the locally weighted scatterplot smoothing method [*Cleveland and Devlin*, 1988]. In this method a smoothed value X_i (corresponding to time t_i) of the time series is calculated by a weighted linear least squares regression of the respective data point and its neighboring points x_{i+k}, where $k = -15, ..., 15$. The length of the smoothing window is constant for all data so that, e.g., in the end points of the time series the regression includes points corresponding to $k = 0, ..., 30$ (series start) or $k = -30, ..., 0$ (series end). The weights are given by the tri-cube weighting function $w_k = \left(1 - \left|\frac{t_i - t_{i+k}}{d(t_i)}\right|^3\right)^3$, where $d(t_i) = \max(t_i - t_{i+k})$ is the maximum time difference between x_i and data points within the smoothing window. The wintertime (December-January-February) temperature anomaly was then calculated in each grid point as the mean of these monthly values, and winters were assigned to the corresponding phase of the sunspot cycle. We excluded grid points having insufficient data coverage with more than 5% of data points missing, in order to have reliable anomaly values over the whole time series. This caused large data gaps in the Arctic Sea, Africa, and China (see Figure 4). The number of winters in 1880–2009 was 17 during
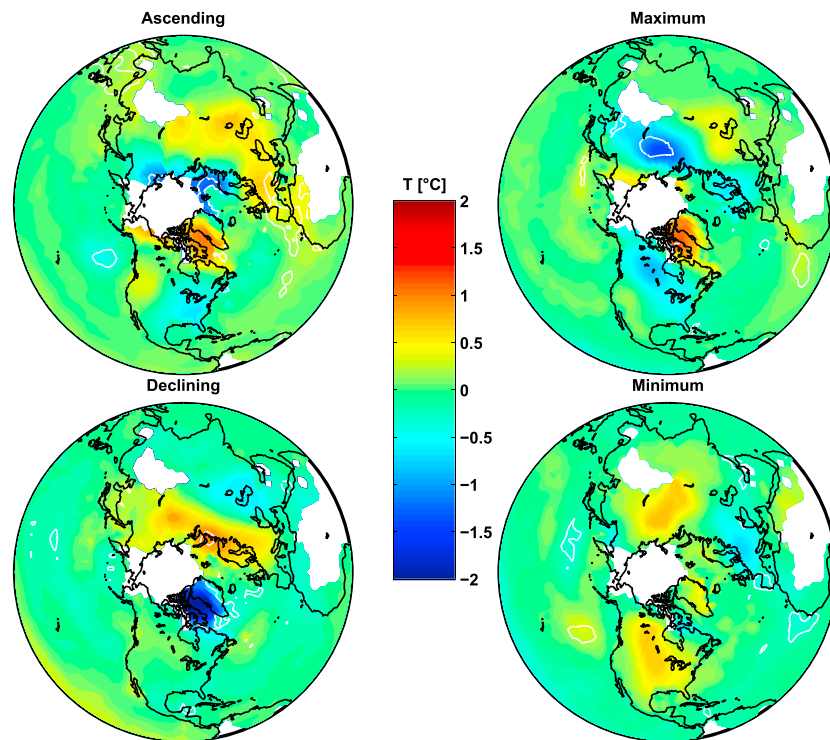
Figure 4. The differences of winter temperature anomalies of each cycle phase and the average of all other winters for solar cycles 12 to 23 (1880–2009). (top left) Ascending phase, (top right) maximum phase, (bottom left) declining phase, and (bottom right) minimum phase. White lines represent 95% confidence level. White areas denote data gaps of grid points with more than 5% of monthly data missing.

ascending phase, 20 during maximum, 25 during declining phase, and 21 during minimum. (These numbers are slightly smaller than in section 3 because the temperature data only cover from cycle 12 (1880) onward.)

Figure 4 shows, for each of the four cycle phases, the spatial pattern of the difference in the mean winter temperature anomalies in the Northern Hemisphere between corresponding cycle phase and the average of all other winters. White lines (within the colored areas) represent 95% confidence levels calculated using the two-sample t test. The confidence levels show whether the differences of the mean winter temperature anomalies in one phase are significantly different from the mean winter temperature anomalies of all other winters. In performing the t test we also took into account the possible temporal autocorrelation of the temperature data. For the winter mean temperatures the autocorrelation was negligible in the continental areas for lags of 1–5 years but moderate in the Pacific and Atlantic regions for 1 year lag (not shown). Thus, we calculated the effective sample sizes [*Von Storch and Zwiers*, 1999] for the t test with lag-1 autocorrelation included. When calculating the effective sample size, the missing values (the grid points where less than 5% of the data points were missing) were interpolated (and excluded in the ends of the time series) so that the autocorrelation function could be defined.

Figure 4 shows that the most distinctive pattern in the temperature differences is found for the declining phase with a significant negative anomaly $-1.7°C$ ($p < 0.01$) in Greenland and a positive anomaly $+1.0°C$ ($p = 0.04$) extending over North Siberia, Scandinavia, and Central Europe. The spatial pattern of temperature anomaly differences for the sunspot maximum phase is roughly opposite to that of the declining phase, but the anomalies are smaller and less systematic and only the negative anomaly of up to $-1.2°C$ ($p = 0.02$) in Northern Siberia is statistically significant. The minimum phase shows weak (not significant) but geographically wide positive difference in temperature anomalies both in North America and North Eurasia and negative difference in the anomalies over most of Europe. The ascending phase mostly resembles the maximum phase, depicting positive (but not significant) difference in the anomalies in Greenland/Baffin Bay area and significant negative difference in the anomalies in Arctic Sea north of Scandinavia. There is also a rather large region extending from Central Europe to Central Asia showing a positive difference in the temperature anomalies.
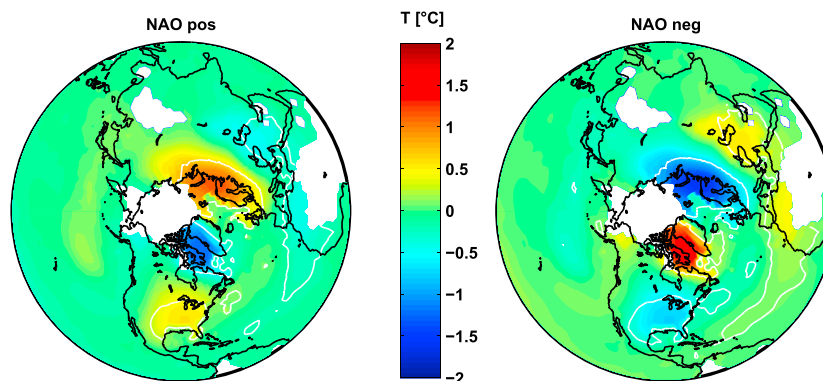
Figure 5. Difference of winter temperature anomalies between (left) positive NAO and overall average and (right) negative NAO and overall average. White lines represent 95% confidence level. White areas denote data gaps of temperature grids with more than 5% of monthly data missing.

Because the statistical significance is estimated separately at each grid point and because of the potentially high spatial correlation in the surface temperature data, it is also necessary to estimate the statistical significance of the entire temperature pattern, i.e., the field significance. We estimated this by using the method proposed by *Livezey and Chen* [1983]. This was done by a Monte Carlo simulation where the winters of the two composites were replaced by an equal number of random years and calculating the percentage of the area k on the spherical surface with a significant difference ($p < 0.05$) in the random composites. The simulation was repeated 10,000 times, and the original observed percentage n was compared to the distribution of k values to get the fraction of k larger than n. The fraction gives the probability of obtaining statistical significance for the percentage n of the considered total area. We found that, if the field significance was calculated by considering the whole Northern Hemisphere, none of the temperature difference patterns were significant at $p < 0.1$, since the results are dominated by the large statistically insignificant areas at low latitudes. However, if we considered only the high latitudes above 50°N, we obtained moderate statistical significance for the declining phase with $p = 0.08$ (i.e., 8% probability that the area determined to be statistically significant at 5% level is obtained by random chance). In all other phases the field significance was significantly lower ($p > 0.3$). This result emphasizes the uniqueness of the declining phase in modulating the winter surface temperatures at high latitudes of the Northern Hemisphere.

The pattern of temperature anomaly differences obtained for the declining phase greatly resembles the pattern of temperature differences between the positive NAO phase and overall average pattern in winter months [e.g., *Hurrell*, 1995; *Hurrell et al.*, 2003]. Figure 5 depicts the difference of the mean temperature anomaly between the positive (left) and negative NAO (right) phases and the overall average temperature anomaly of the winter months in 1880–2009. (The total mean of the winter time NAO index over the whole interval was 0.05, i.e., slightly positive.) One can see that the two plots in Figure 5 are practically mirror images of each other. The white lines represent 95% confidence levels calculated similarly as above but now comparing positive and negative NAO winters separately to the overall winter average. The positive NAO pattern has a negative temperature anomaly in Greenland and a weaker (but still significant) negative anomaly in the Middle East, and a large positive anomaly region covering Scandinavia, Central Europe, Northern Siberia and a weaker (but also significant) positive anomaly region in eastern North America. These are all opposite to the (also significant) anomalies found during the negative NAO phase. Figures 4 and 5 depict the great similarity of the patterns during the declining phase and the positive NAO. The pattern in the sunspot maximum phase and also in the ascending phase resembles the negative NAO pattern, but the significance of the anomalies is weaker, as mentioned above.

5. NAO Variability During Different Phases of the Sunspot Cycle

The similarity in the patterns depicted in Figures 4 and 5 suggests that the positive NAO occurs more frequently during the declining phase than in other cycle phases. This is also consistent with earlier studies finding positive correlation between geomagnetic activity/solar wind speed/precipitating electrons (see also Figure 3) and the NAO index [*Boberg and Lundstedt*, 2003; *Thejll et al.*, 2003; *Bochníček and Hejda*, 2005;
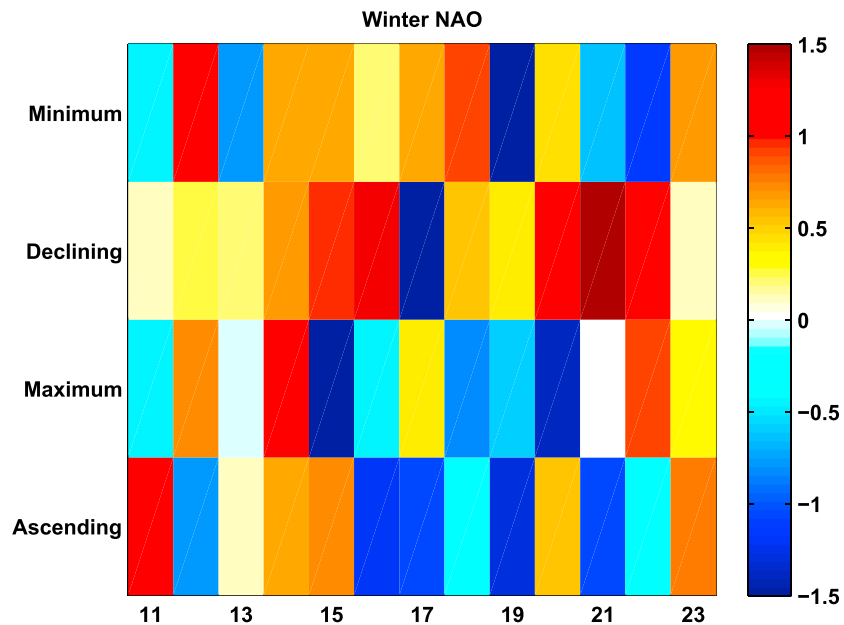
Figure 6. Mean winter NAO index during the four cycle phases for cycles 11 to 23 in color coding. Cycle phases are given in the vertical axis and cycle numbers in the horizontal axis.

Maliniemi et al., 2013]. On the other hand, there are also indications of strengthening of the NAO pattern related to sunspots/solar $F_{10.7}$ cm [e.g., *Kodera*, 2002; *Huth et al.*, 2006; *Ineson et al.*, 2011].

We have studied the NAO variability during the four different sunspot cycle phases by computing the average wintertime NAO index separately for each cycle phase and for each solar cycle. Figure 6 shows that the NAO index is positive during the declining phase of all but one solar cycle (cycle 17). During the other phases the NAO index is less systematic having roughly equal number of cycles with negative and positive NAO values in each phase. Strong correlation between geomagnetic activity and NAO [*Thejll et al.*, 2003; *Bochníček and Hejda*, 2005] for the latter half of the twentieth century is indicated by the strongly positive NAO in the declining phase and negative NAO in the minimum phase for cycles 19 to 22 (see also Figure 3).

Figure 6 shows that the maximum phase has a positive NAO for the last two cycles, but mostly negative before that. Some earlier studies have found that the difference of the sea level pressure patterns between the solar maximum and minimum resembles the positive NAO pattern [e.g., *Kodera*, 2002; *Ineson et al.*, 2011]. *Kodera* [2002] studied solar cycles 20 to 22 and defined the solar maximum (minimum) as years with larger (smaller) $F_{10.7}$ cm solar flux than the overall average. *Ineson et al.* [2011], on the other hand, defined the solar maximum and minimum as a lower and upper third of the open solar flux for years 1957 to 2010. To compare our results to these previous studies, we also studied (not shown) how the temperature patterns and NAO index were distributed if we used a shorter time interval covering cycles 19 to 23, roughly corresponding the time interval in earlier studies [*Kodera*, 2002; *Huth et al.*, 2006; *Ineson et al.*, 2011]. We found that if we split the phase function into two halves (maximum 90° − 270° and minimum 270° − 90°), we got a slightly positive average NAO (0.10) in the maximum and negative NAO (−0.20) in the minimum. The differences in the temperature anomaly patterns also slightly resembled the positive NAO pattern in the maximum and negative NAO pattern in the minimum but without statistical significance. On the other hand, we must also note that these earlier studies used either sea level pressure or tropospheric geopotential height, not the station-based NAO index we used. As stated earlier, the station-based NAO index does not include the movement of the pressure centers. It is also known that the surface temperature variability related to NAO varies over time [*Chen and Hellström*, 1999; *Jung et al.*, 2003]. These differences, including the different definitions of the winter season (March was included among winter months in *Kodera* [2002] and *Huth et al.* [2006]) and the different definition of solar activity levels or solar cycle phases, likely explain the differences in these results.

Recent results concerning longer-term sea level pressure variability related to the solar activity show features that mostly agree with our results. *Gray et al.* [2013] showed that during solar maximum and ascending
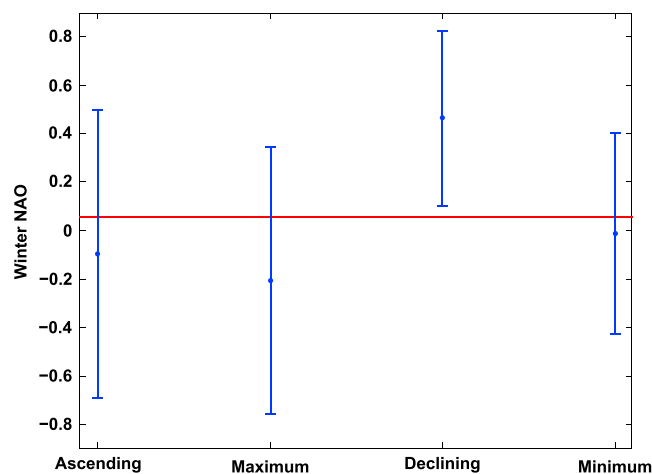
Figure 7. Mean winter NAO index values for the four cycle phases, averaged over cycles 11 to 23. The red line represents the overall mean value of wintertime NAO (0.05). Bars represent the 95% confidence intervals.

phase (0 year lag and 8–10 year lag to the solar maximum year) sea level pressure field resembled negative NAO and during the declining phase (2–4 years lag) the pressure field resembled positive NAO. In their longer-term study extending back to the sixteenth century, *Brugnara et al.* [2013] also found differences in the North Atlantic and European wintertime (defined as January, February, and March) sea level pressure between solar maximum and minimum, but they stated it as not being related to the NAO but rather to the Eurasian pattern [*Barnston and Livezey*, 1987].

Figure 7 depicts the mean NAO index during each cycle phase averaged over cycles 11 to 23. The error bars represent 95% confidence intervals obtained by the t test. We note that temporal autocorrelation of the mean winter NAO is very small (<0.1 for 1–10 year lags) and can be neglected when computing the confidence intervals. The red line represents the overall mean wintertime NAO (0.05). Figure 7 verifies the unique nature of the declining phase, the only phase having a mean NAO index (0.46 ± 0.36), which is statistically significantly different from the long-term mean. We note that although the maximum phase has the largest negative mean NAO (-0.20 ± 0.55), which is in agreement with the results depicted in Figure 4, it is not statistically different from the long-term mean. Mean wintertime NAO values during the ascending and minimum phases are close to the long-term mean.

6. Temperature Anomalies During Weak Cycles in 1880–1925

The mean wintertime NAO averaged over cycles 12 to 15 (see Figure 6) was positive for nearly all the four cycle phases (especially clear in cycles 14 and 15). These cycles were weaker in sunspot activity than the other solar cycles during the last 130 years (see Figure 1). To study this period in more detail, we have shown the mean winter surface temperature anomalies over these four cycles for the different cycle phases in Figure 8. The number of winter months was now seven for ascending phase, nine for maximum phase, eight for declining phase, and seven for minimum phase. (It should be noted that during these early cycles the coverage of weather stations contributing to the data series was more sparse than in later times.)

Roughly the same temperature patterns emerge for the different cycle phases as in Figure 4. Most notably, the declining phase shows again a very clear positive NAO pattern with a strongly significant negative temperature anomaly in Greenland and a positive temperature anomaly in Europe and Siberia. Minimum phase shows a similar overall pattern in Figure 8 as in Figure 4 with positive (but not significant) temperature anomaly in both North America and Eurasia. A significant positive temperature anomaly appears in Figure 8 in Western Russia in the ascending phase, the pattern resembling closely the ascending phase in Figure 4. A negative temperature anomaly appears in North Canada in the maximum phase, in partial similarity with the positive NAO pattern.

Field significance test for the high latitudes above 50°N yields moderate significance ($p = 0.07$) for the positive NAO pattern in the declining phase, while all other phases remain statistically insignificant ($p > 0.3$). These results further emphasize the unique relation between the positive NAO at high latitudes and the declining phase of the sunspot cycle. Figure 8 shows, most interestingly, that this close relation does not depend on the overall level of solar activity, i.e., the height of the sunspot cycles, but is consistent for both the weak cycles at the turn of nineteenth/twentieth century and for the active cycles in the second half of the twentieth century.
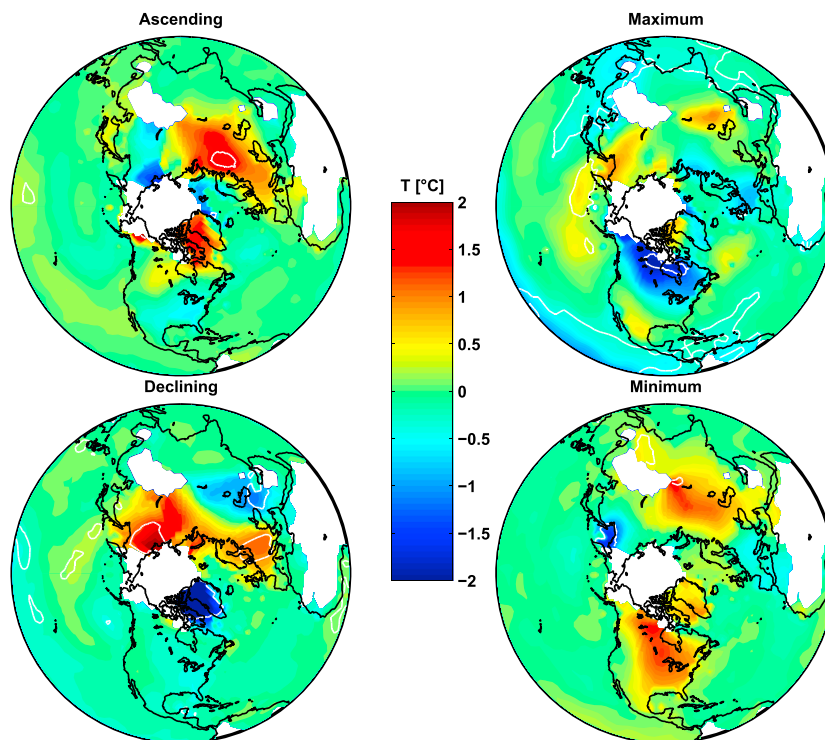
Figure 8. Same as in Figure 4 but using data for cycles 12 to 15 only (1880–1925).

7. Discussion and Conclusions

We have shown that the different phases of the sunspot cycle have a different effect on winter surface temperatures in the Northern Hemisphere and on the NAO index. By defining a sunspot cycle phase function in terms of the official sunspot maximum and minimum times, we showed that the declining phase of the sunspot cycle remarkably consistently produces the spatial pattern of surface temperature anomalies related to the positive NAO during the last 13 solar cycles. We also showed that the close similarity between the surface temperature patterns in the declining phase and during the positive NAO does not depend on the overall sunspot activity level but remains essentially the same during both the weak solar cycles at the turn of nineteenth/twentieth century and during active solar cycles in the latter half of the twentieth century. We found that the maximum phase and ascending phase of the cycle have, on an average, a negative wintertime NAO index and a temperature pattern, which slightly resembles the negative NAO pattern. However, this connection is based on weaker statistical significance and depicts considerable variability with overall sunspot activity over long time scales.

We also studied the distribution of several suggested solar-related climate drivers in the four cycle phases and showed explicitly that only solar wind speed and energetic electron precipitation have their maxima in the declining phase of the solar cycle, as defined here. Some earlier studies have shown that the NAO index correlates positively with these parameters and geomagnetic activity during winter [*Boberg and Lundstedt*, 2003; *Thejll et al.*, 2003; *Bochníček and Hejda*, 2005; *Maliniemi et al.*, 2013]. However, other studies have suggested strengthening of the NAO pattern related to the solar maxima [*Kodera*, 2002; *Huth et al.*, 2006; *Ineson et al.*, 2011]. Our results do not show a significant NAO response in the solar maximum. Possible reasons for this difference may be the methodological differences including the definition of NAO (principal component based versus pressure difference of stations), differences in temporal coverage, and in the mixing of different solar activity levels and solar cycle phases. On the other hand, our results agree well with the recent results obtained by *Gray et al.* [2013] who found sea level pressure variability related to the solar cycle to resemble the positive NAO pattern with a 2–4 years lag to the solar maximum when roughly the same time period was used.

The results obtained here give support to the mechanism suggested by *Baumgaertner et al.* [2011] in a chemistry-climate model where enhanced geomagnetic activity/energetic particle precipitation leads to

the destruction of stratospheric ozone and strengthening of the northern annular mode. Because the energetic particle precipitation peaks typically in the declining phase 3–4 years after the sunspot maximum, the observed lag between the NAO/surface temperature pattern and the sunspot cycle arises quite naturally in this mechanism. Recently, *Scaife et al.* [2013] suggested an alternative mechanism based on a general circulation model, where a sudden step-like change in the solar UV forcing can cause sea level pressure signature to build up during several years when the Atlantic Ocean acts as a heat buffer to the solar UV forcing. They concluded that the modeled feedback, while present, appeared to be too weak to explain the observed lag. Using Hadley Center Sea Level Pressure data, *Gray et al.* [2013] observed a lag in the sea level pressure response of 2–4 years following solar maximum. However, using the same model as *Scaife et al.* [2013] with a realistic variation of solar irradiance over the solar cycle, they confirmed that the model response did not produce strong enough lag to explain the observations. Although the lag is currently not well explained by the solar UV forcing in the general circulation models, we note that a more complete picture of the different mechanisms and their effects would require a sophisticated model with realistic inputs of solar irradiance and energetic particle precipitation. This would be important in order to estimate the relative strength of the different drivers and couplings in the North Atlantic region. Nevertheless, the results presented here will improve our current understanding of winter circulation and surface temperature modulation by the solar-related parameters, which is very valuable for both atmospheric/climate and space physics communities.

References

Asikainen, T., and K. Mursula (2013), Correcting the NOAA/MEPED energetic electron fluxes for detector efficiency and proton contamination, *J. Geophys. Res. Space Physics*, *118*, 6500–6510, doi:10.1002/jgra.50584.

Baldwin, M. P., and T. J. Dunkerton (2001), Stratospheric harbingers of anomalous weather regimes, *Science*, *294*, 581–584, doi:10.1126/science.1063315.

Barnston, A. G., and R. E. Livezey (1987), Classification, seasonality and persistence of low-frequency atmospheric circulation patterns, *Mon. Weather Rev.*, *115*, 1083–1126, doi:10.1175/1520-0493(1987)115<1083:CSAPOL>2.0.CO;2.

Barriopedro, D., R. García-Herrera, and R. Huth (2008), Solar modulation of Northern Hemisphere winter blocking, *J. Geophys. Res.*, *113*, D14118, doi:10.1029/2008JD009789.

Baumgaertner, A. J. G., A. Seppälä, P. Jöckel, and M. A. Clilverd (2011), Geomagnetic activity related NOₓ enhancements and polar surface air temperature variability in a chemistry climate model: Modulation of the NAM index, *Atmos. Chem. Phys.*, *11*, 4521–4531, doi:10.5194/acp-11-4521-2011.

Boberg, F., and H. Lundstedt (2003), Solar wind electric field modulation of the NAO: A correlation analysis in the lower atmosphere, *Geophys. Res. Lett.*, *30*(15), 1825, doi:10.1029/2003GL017360.

Bochníček, J., and P. Hejda (2005), The winter NAO pattern changes in association with solar and geomagnetic activity, *J. Atmos. Sol. Terr. Phys.*, *67*, 17–32, doi:10.1016/j.jastp.2004.07.014.

Bochníček, J., H. Davídkovová, P. Hejda, and R. Huth (2012), Circulation changes in the winter lower atmosphere and long-lasting solar/geomagnetic activity, *Ann. Geophys.*, *30*, 1719–1726, doi:10.5194/angeo-30-1719-2012.

Brugnara, Y., S. Brönnimann, J. Luterbacher, and E. Rozanov (2013), Influence of the sunspot cycle on the Northern Hemisphere wintertime circulation from long upper-air data sets, *Atmos. Chem. Phys.*, *13*, 6275–6288, doi:10.5194/acp-13-6275-2013.

Calisto, M., I. Usoskin, E. Rozanov, and T. Peter (2011), Influence of galactic cosmic rays on atmospheric composition and dynamics, *Atmos. Chem. Phys.*, *11*, 4547–4556, doi:10.5194/acp-11-4547-2011.

Chen, D., and C. Hellström (1999), The influence of the North Atlantic oscillation on the regional temperature variability in Sweden: Spatial and temporal variations, *Tellus Ser. A*, *51*, 505–516, doi:10.1034/j.1600-0870.1999.t01-4-00004.x.

Cleveland, W. S., and S. J. Devlin (1988), Locally-weighted regression: An approach to regression analysis by local fitting, *J. Am. Stat. Assoc.*, *83*, 596–610, doi:10.2307/2289282.

Echer, E., W. D. Gonzalez, A. L. C. Gonzalez, A. Prestes, L. E. A. Vieira, A. dal Lago, F. L. Guarnieri, and N. J. Schuch (2004), Long-term correlation between solar and geomagnetic activity, *J. Atmos. Sol. Terr. Phys.*, *66*, 1019–1025, doi:10.1016/j.jastp.2004.03.011.

Ermolli, I., et al. (2013), Recent variability of the solar spectral irradiance and its impact on climate modelling, *Atmos. Chem. Phys.*, *13*, 3945–3977, doi:10.5194/acp-13-3945-2013.

Funke, B., M. López-Puertas, S. Gil-López, T. von Clarmann, G. P. Stiller, H. Fischer, and S. Kellmann (2005), Downward transport of upper atmospheric NOₓ into the polar stratosphere and lower mesosphere during the Antarctic 2003 and Arctic 2002/2003 winters, *J. Geophys. Res.*, *110*, D24308, doi:10.1029/2005JD006463.

Georgieva, K., B. Kirov, and E. Gavruseva (2006), Geoeffectiveness of different solar drivers, and long-term variations of the correlation between sunspot and geomagnetic activity, *Phys. Chem. Earth*, *31*, 81–87, doi:10.1016/j.pce.2005.03.003.

Gray, L. J., et al. (2010), Solar influences on climate, *Rev. Geophys.*, *48*, RG4001, doi:10.1029/2009RG000282.

Gray, L. J., et al. (2013), A lagged response to the 11 year solar cycle in observed winter Atlantic/European weather patterns, *J. Geophys. Res. Atmos.*, *118*, 13,405–13,420, doi:10.1002/2013JD020062.

Hansen, J., R. Ruedy, M. Sato, and K. Lo (2010), Global surface temperature change, *Rev. Geophys.*, *48*, RG4004, doi:10.1029/2010RG000345.

Hurrell, J. W. (1995), Decadal trends in the North Atlantic oscillation: Regional temperatures and precipitation, *Science*, *269*, 676–679, doi:10.1126/science.269.5224.676.

Hurrell, J. W., and C. Deser (2009), North Atlantic climate variability: The role of the North Atlantic oscillation, *J. Mar. Syst.*, *78*, 28–41, doi:10.1016/j.jmarsys.2008.11.026.

Hurrell, J. W., Y. Kushnir, G. Ottersen, and M. Visbeck (2003), *The North Atlantic Oscillation: Climate Significance and Environmental Impact*, *Geophys. Monog. Ser.*, vol. 134, pp. 1–36, AGU, Washington D. C., doi:10.1029/134GM01.

Huth, R., L. Pokorná, J. Bochníček, and P. Hejda (2006), Solar cycle effects on modes of low-frequency circulation variability, *J. Geophys. Res.*, *111*, D22107, doi:10.1029/2005JD006813.

Huth, R., J. Kyselý, J. Bochníček, and P. Hejda (2008), Solar activity affects the occurrence of synoptic types over Europe, *Ann. Geophys.*, *26*, 1999–2004, doi:10.5194/angeo-26-1999-2008.

Ineson, S., A. A. Scaife, J. R. Knight, J. C. Manners, N. J. Dunstone, L. J. Gray, and J. D. Haigh (2011), Solar forcing of winter climate variability in the Northern Hemisphere, *Nat. Geosci.*, *4*, 753–757, doi:10.1038/ngeo1282.

Jung, T., M. Hilmer, E. Ruprecht, S. Kleppek, S. K. Gulev, and O. Zolina (2003), Characteristics of the recent eastward shift of interannual NAO variability, *J. Clim.*, *16*, 3371–3382, doi:10.1175/1520-0442(2003)016<3371:COTRES>2.0.CO;2.

Kodera, K. (2002), Solar cycle modulation of the North Atlantic oscillation: Implication in the spatial structure of the NAO, *Geophys. Res. Lett.*, *29*(8), 1218, doi:10.1029/2001GL014557.

Kodera, K., and Y. Kuroda (2002), Dynamical response to the solar cycle, *J. Geophys. Res.*, *107*, 4749, doi:10.1029/2002JD002224.

Konopka, P., et al. (2007), Ozone loss driven by nitrogen oxides and triggered by stratospheric warmings can outweigh the effect of halogens, *J. Geophys. Res.*, *112*, D05105, doi:10.1029/2006JD007064.

Krivova, N. A., L. E. A. Vieira, and S. K. Solanki (2010), Reconstruction of solar spectral irradiance since the Maunder minimum, *J. Geophys. Res.*, *115*, A12112, doi:10.1029/2010JA015431.

Labitzke, K. (2005), On the solar cycle QBO relationship: A summary, *J. Atmos. Sol. Terr. Phys.*, *67*, 45–54, doi:10.1016/j.jastp.2004.07.016.

Leske, R. A., A. C. Cummings, R. A. Mewaldt, and E. C. Stone (2013), Anomalous and galactic cosmic rays at 1 AU during the cycle 23/24 solar minimum, *Space Sci. Rev.*, *176*, 253–263, doi:10.1007/s11214-011-9772-1.

Li, Y., H. Lu, M. J. Jarvis, M. A. Clilverd, and B. Bates (2011), Nonlinear and nonstationary influences of geomagnetic activity on the winter North Atlantic Oscillation, *J. Geophys. Res.*, *116*, D16109, doi:10.1029/2011JD015822.

Livezey, R. E., and W. Y. Chen (1983), Statistical field significance and its determination by Monte Carlo techniques, *Mon. Weather Rev.*, *111*, 46–59, doi:10.1175/1520-0493(1983)111<0046:SFSAID>2.0.CO;2.

Lockwood, M., R. G. Harrison, T. Woollings, and S. K. Solanki (2010), Are cold winters in Europe associated with low solar activity?, *Environ. Res. Lett.*, *5*(2), 024,001, doi:10.1088/1748-9326/5/2/024001.

Lu, H., M. J. Jarvis, H.-F. Graf, P. C. Young, and R. B. Horne (2007), Atmospheric temperature responses to solar irradiance and geomagnetic activity, *J. Geophys. Res.*, *112*, D11109, doi:10.1029/2006JD007864.

Lu, H., M. J. Jarvis, and R. E. Hibbins (2008), Possible solar wind effect on the northern annular mode and northern hemispheric circulation during winter and spring, *J. Geophys. Res.*, *113*, D23104, doi:10.1029/2008JD010848.

Maliniemi, V., T. Asikainen, K. Mursula, and A. Seppälä (2013), QBO-dependent relation between electron precipitation and wintertime surface temperature, *J. Geophys. Res. Atmos.*, *118*, doi:10.1002/jgrd.50518.

Matthes, K., U. Langematz, L. L. Gray, K. Kodera, and K. Labitzke (2004), Improved 11-year solar signal in the Freie Universität Berlin Climate Middle Atmosphere Model (FUB-CMAM), *J. Geophys. Res.*, *109*, D06101, doi:10.1029/2003JD004012.

Matthes, K., Y. Kuroda, K. Kodera, and U. Langematz (2006), Transfer of the solar signal from the stratosphere to the troposphere: Northern winter, *J. Geophys. Res.*, *111*, D06108, doi:10.1029/2005JD006283.

McCormack, J. P., and L. L. Hood (1996), Apparent solar cycle variations of upper stratospheric ozone and temperature: Latitude and seasonal dependences, *J. Geophys. Res.*, *101*, 20,933–20,944, doi:10.1029/96JD01817.

Meehl, G. A., J. M. Arblaster, G. Branstator, and H. van Loon (2008), A coupled air sea response mechanism to solar forcing in the Pacific region, *J. Clim.*, *21*, 2883–2897, doi:10.1175/2007JCLI1776.1.

Mironova, I., B. Tinsley, and L. Zhou (2012), The links between atmospheric vorticity, radiation belt electrons, and the solar wind, *Adv. Space Res.*, *50*, 783–790, doi:10.1016/j.asr.2011.03.043.

Randall, C. E., et al. (2005), Stratospheric effects of energetic particle precipitation in 2003-2004, *Geophys. Res. Lett.*, *32*, L05802, doi:10.1029/2004GL022003.

Roy, I., and J. D. Haigh (2012), Solar cycle signals in the Pacific and the issue of timings, *J. Atmos. Sci.*, *69*, 1446–1451, doi:10.1175/JAS-D-11-0277.1.

Rozanov, E., L. Callis, M. Schlesinger, F. Yang, N. Andronova, and V. Zubov (2005), Atmospheric response to NO_y source due to energetic electron precipitation, *Geophys. Res. Lett.*, *32*, L14811, doi:10.1029/2005GL023041.

Rozanov, E., M. Calisto, T. Egorova, T. Peter, and W. Schmutz (2012), Influence of the precipitating energetic particles on atmospheric chemistry and climate, *Surv. Geophys.*, *33*(3), 483–501.

Scaife, A. A., S. Ineson, J. R. Knight, L. Gray, K. Kodera, and D. M. Smith (2013), A mechanism for lagged North Atlantic climate response to solar variability, *Geophys. Res. Lett.*, *40*, 434–439, doi:10.1002/grl.50099.

Seppälä, A., P. T. Verronen, M. A. Clilverd, C. E. Randall, J. Tamminen, V. Sofieva, L. Backman, and E. Kyrölä (2007), Arctic and Antarctic polar winter NO_x and energetic particle precipitation in 2002-2006, *Geophys. Res. Lett.*, *34*, L12810, doi:10.1029/2007GL029733.

Seppälä, A., C. E. Randall, M. A. Clilverd, E. Rozanov, and C. J. Rodger (2009), Geomagnetic activity and polar surface air temperature variability, *J. Geophys. Res.*, *114*, A10312, doi:10.1029/2008JA014029.

Seppälä, A., H. Lu, M. A. Clilverd, and C. J. Rodger (2013), Geomagnetic activity signatures in wintertime stratosphere wind, temperature, and wave response, *J. Geophys. Res. Atmos.*, *118*, 2169–2183, doi:10.1002/jgrd.50236.

Sinnhuber, M., S. Kazeminejad, and J. M. Wissing (2011), Interannual variation of NO_x from the lower thermosphere to the upper stratosphere in the years 1991-2005, *J. Geophys. Res.*, *116*, A02312, doi:10.1029/2010JA015825.

Smith, E. J., and A. Balogh (2008), Decrease in heliospheric magnetic flux in this solar minimum: Recent Ulysses magnetic field observations, *Geophys. Res. Lett.*, *35*, L22103, doi:10.1029/2008GL035345.

Thejll, P., B. Christiansen, and H. Gleisner (2003), On correlations between the North Atlantic oscillation, geopotential heights, and geomagnetic activity, *Geophys. Res. Lett.*, *30*(6), 1347, doi:10.1029/2002GL016598.

Tinsley, B. A. (2000), Influence of solar wind on the global electric circuit, and inferred effects on cloud microphysics, temperature, and dynamics in the troposphere, *Space Sci. Rev.*, *94*, 231–258.

Veretenenko, S. V., V. A. Dergachev, and P. B. Dmitriyev (2005), Long-term variations of the surface pressure in the North Atlantic and possible association with solar activity and galactic cosmic rays, *Adv. Space Res.*, *35*, 484–490, doi:10.1016/j.asr.2005.04.004.

van Loon, H., and K. Labitzke (1988), Association between the 11-year solar cycle, the QBO, and the atmosphere. Part II: Surface and 700 mb in the Northern Hemisphere in winter, *J. Clim.*, *1*, 905–920, doi:10.1175/1520-0442(1988)001<0905:ABTYSC>2.0.CO;2.

Von Storch, H., and F. W. Zwiers (1999), *Statistical Analysis in Climate Research*, Cambridge Univ. Press, Cambridge, U. K.

Wang, Y.-H., G. Magnusdottir, H. Stern, X. Tian, and Y. Yu (2012), Decadal variability of the NAO: Introducing an augmented NAO index, *Geophys. Res. Lett.*, *39*, L21702, doi:10.1029/2012GL053413.

Woollings, T., M. Lockwood, G. Masato, C. Bell, and L. Gray (2010), Enhanced signature of solar variability in Eurasian winter climate, *Geophys. Res. Lett.*, *37*, L20805, doi:10.1029/2010GL044601.